Applied Thermal Engineering xxx (xxxx) xxx

Contents lists available at ScienceDirect

Applied Thermal Engineering

journal homepage: www.elsevier.com/locate/apthermeng

Optimized sorber bed heat and mass exchangers for sorption cooling systems

Hesam Bahrehmand, Majid Bahrami *

Laboratory for Alternative Energy Conversion (LAEC), School of Mechatronic Systems Engineering, Simon Fraser University, Surrey, BC V3T 0A3, Canada

ARTICLE INFO

Keywords:
Optimized sorber bed
Sorption cooling systems
Analytical modeling
Analysis of variance
Specific cooling power
Coefficient of performance

ABSTRACT

Low sorbent thermal diffusivity and off-the-shelf design of sorber beds have impeded the wide market adoption of sorption systems. In this study, graphite flakes are added to the sorbent to increase the thermal diffusivity and sorber beds are specifically designed and optimized for sorption systems. First, an analysis of variance is carried out to find the key parameters of sorber beds using the developed 2-D analytical models. It is shown that all components of the sorber bed, namely the sorbent, heat exchanger and heat transfer fluid, should be optimized simultaneously. Moreover, the specific cooling power (SCP) and coefficient of performance (COP) should be optimized simultaneously due to their conflicting trends. Thus, using the developed analytical models and multi-objective genetic algorithm, an optimization study is conducted. Based on the optimization results, two new sorber beds of finned-tube sorber bed heat and mass exchanger (F-HMX) and plate-fin sorber bed heat and mass exchanger (P-HMX) are designed, built, and tested in our custom-built two-sorber bed sorption test bed. The experimental results show that the present P-HMX can achieve an SCP of 1,005 W/kg sorbent, and a COP of 0.60 which are higher than the previously published results in the literature. Furthermore, the F-HMX design yields an SCP of 766 W/kg and a COP of 0.55. It is shown that the P-HMX, which is specifically designed and optimized for sorption cooling systems, provides up to 4.3 times higher SCP, and 3 times higher COP compared to an off-the-shelf heat exchanger, an engine oil cooler coated with a similar composite sorbent consisting of $CaCl_2$, silica gel B150 and PVA. The present P-HMX has been tested under a wide range of operating conditions: i) desorption temperature (60–90 °C); ii) sorption and condenser temperatures (20–40 °C); iii) evaporator temperature (5–20 °C); and iv) cycle time (10–20 min). The SCP in the range of 320–1,230 W/kg and COP of 0.40–0.80 are measured in our test bed over the targeted operating conditions.

1. Introduction

The global cooling energy demand is expected to triple by 2050, requiring new electricity capacity equivalent to the combined electricity capacity of the US, EU and Japan today [1]. Furthermore, the share of cooling in electricity peak loads is anticipated to increase, particularly in hot countries like India – where the share of air conditioning (AC) in peak electricity load could reach 45% in 2050, up from 10% today [1,2]. This increase in electricity peak load would require USD $3.183 trillion investments in power generation and electrical grid [2]. However, advancements in cooling technology could lead to substantial reduction in the peak load, and hence, the required investments in new power plants and the electrical grid by 38% [2]. Advancements in cooling technology include: (i) performance enhancement of the current cooling technologies; and (ii) development of cooling technologies powered with energy sources other than electricity.

Vapor compression refrigeration (VCR) is currently the most used technology meeting market requirements [3], forming 99% of space-cooling energy consumption in the US [4]. However, VCR is powered by electricity, which is produced predominantly from fossil fuels, up to 76% globally [5]. Moreover, VCR employs fluorocarbon refrigerants that contribute to climate change because of their greenhouse gas (GHG) effects. VCR systems contribute to about 10% of GHG emissions globally [6].

Sorption cooling systems (SCS) can be powered with low-grade thermal energy, i.e. heat sources with temperature<100 °C, such as waste heat and solar energy. Low-grade thermal energy is non-payable and abundant in different sectors [5]. In addition to cooling, sorption systems have shown potential for other applications, including heat pumping, heat upgrading, thermal energy storage, desalination, dehumidification and gas separation. The advantages of SCS are non-

* Corresponding author at: School of Mechatronic Systems Engineering, Simon Fraser University, 250-13450 102 Avenue, Surrey, BC V3T 0A3, Canada.
E-mail addresses: sbahrehm@sfu.ca (H. Bahrehmand), mbahrami@sfu.ca (M. Bahrami).

https://doi.org/10.1016/j.applthermaleng.2020.116348
Received 18 April 2020; Received in revised form 30 October 2020; Accepted 16 November 2020
Available online 21 November 2020

Nomenclature

b	Fin height, m
c_p	Specific heat capacity, J/kgK
h_{fg}	Enthalpy of evaporation, J/kg
H_c	Channel height, m
m	Mass, kg
p	Pressure, Pa
p_0	Saturation pressure, Pa
Q	Energy, J
r	Fluid tube radius
T	Temperature, K
t	Time (s), thickness (m)

Greek symbols

τ	Cycle time, s
ϕ	Graphite flake content in the sorbent, wt.%
ω	Sorbate uptake (g H_2O/g dry sorbent)

Subscripts

c	Fluid channel
cond	Condenser
des	Desorption
evap	Evaporator/evaporative
eq	Equilibrium
f	Fin
sat	Saturation
s, sorb	Sorbent
sorp	Sorption

Abbreviations

ANOVA	Analysis of variance
CEC	Combined evaporator and condenser
COP	Coefficient of performance
HEX	Heat exchanger
HR	Heat recovery
HTF	Heat transfer fluid
IEA	International energy agency
LGTE	Low-grade thermal energy
F-HMX	Finned-tube sorber bed heat exchanger
P-HMX	Plate-fin sorber bed heat exchanger
SCP	Specific cooling power
S-HMX	Sorber bed heat exchanger
SWS	Selective water sorbent
TCP	Total cooling power
TCS	Temperature control system
VSCP	Volumetric specific cooling power

corrosive, non-toxic and environmentally-friendly sorption pairs with zero ozone depletion potential (ODP) and zero global warming potential (GWP), low desorption temperature, no moving parts, low noise level, low electricity consumption and low maintenance [7–9]. Nevertheless, the major disadvantages are low COP because of temperature swing between sorption and desorption and large size. The specific cooling power (SCP) per total mass of the system for SCS is 15.9–45.4 W/kg [10–15], versus 113–160 W/kg for VCR [16–18]. Such low SCP of SCS would result in heavy and bulky systems, which is the main impediment against the wide adoption of SCS. This paper aims to address two major limitations of sorption systems, namely:

i. low specific cooling power (SCP), resulting from low sorbent thermal diffusivity and the use of off-the-shelf heat exchanger designs. High porosity of the sorbent materials, which is crucial for sorption mass transfer, results in low thermal conductivity that impedes their heat transfer. Furthermore, the off-the-shelf heat exchangers commonly used as the sorber bed heat and mass exchanger (S-HMX), such as radiators and coolers, are not designed and optimized for sorption systems and limit their performance;
ii. low coefficient of performance (COP), in part due to the high thermal inertia of the currently used off-the-shelf heat exchangers in sorption systems.

These issues are addressed by providing a new analytical approach for design and optimization of S-HMX for sorption systems, while minimizing their thermal inertia.

Table 1 presents a summary of available studies in which optimization was conducted on the operating conditions and/or sorber bed heat exchanger design. Most studies optimize the variables and/or objective functions in an asynchronous manner, while the optimization should be performed simultaneously. In addition, the available studies with simultaneous optimization have not optimized all the S-HMX components, i.e., sorbent, heat exchanger and heat transfer fluid.

Many researchers have developed sorber bed heat and mass exchangers (S-HMXs) to tackle the issue of low performance of sorption cooling systems (SCS). A summary of the available studies with a compromise between specific cooling power (SCP) and the coefficient of performance (COP) is presented in Table 2. The performance has been enhanced considerably over the past decade; however, most of the performance enhancement can be attributed to the utilization of zeolite-based sorbents, such as SAPO-34 and AQSOA FAM Z02, which are rather expensive, due to their synthesis process [38]. Furthermore, majority of uptake in zeolite-based sorbents occurs in a narrow range of relative pressure, p/p_0, which may limit their application to relatively high desorption temperature, i.e. heat source of 80–90 °C, and low condenser temperature, i.e. about 30 °C. The objective of this study is to develop an S-HMX that provides a high SCP and COP over a large range of operating conditions.

In the present study, the geometrical, heat transfer characteristics and cycle time of the S-HMX are optimized simultaneously to achieve an optimal SCP and COP concurrently. To achieve this objective, first, an analysis of variance (ANOVA) is conducted to find the level of contribution of each parameter to the performance of the SCS. Subsequently, a simultaneous multi-objective optimization study is carried out to obtain a set of optimum solutions for SCP and COP.

The sorbent material used is comprised of silica gel as the porous host matrix impregnated with $CaCl_2$, and graphite flakes as thermally-conductive additives and PVA as the binder. In this paper, the material is called “sorbent” and the phenomenon is called “sorption” due to the simultaneous adsorption by silica gel and absorption by $CaCl_2$. It should be noted that these composite sorbents have a lower cost and a higher market availability compared to the zeolite-based sorbents [39]. Moreover, the sorption performance of these composites takes place over the entire range of relative pressure, $0.06 < p/p_0 < 0.4$, which is more appropriate for air-conditioning applications [40].

2. Performance parameters

Specific cooling power (SCP) is defined as the ratio of evaporative cooling energy to the product of cycle time and dry sorbent mass, Eq. (1). The SCP shows how fast the cooling energy can be delivered and how compact the sorption system is. For an SCS with an ideal evaporator and condenser, SCP can be increased by enhancing the heat and mass transfer processes in S-HMX. See Fig. A1 and Fig. A2 in Appendix A for a schematic of the S-HMX and parameters.

Table 1
Summary of the existing studies on optimization of sorption cooling systems.

Ref. No.	Optimization variables	Objective functions	Optimization type
[19]	• Fin pitch fin length	• Differential sorbate uptake	Asynchronous
[20]	• Cycle time Adsorption to desorption time	• SCP COP	Simultaneous
[21]	• Adsorber diameter	• Differential sorbate uptake COP	Asynchronous
[22]	• Cycle time Mass recovery time	• SCP COP	Asynchronous
[23]	• Desorption temperature Cooling temperature Heat transfer fluid flow rate Adsorption to desorption time Mass recovery time Heat recovery time	• SCP COP	Asynchronous
[24]	• Fin pitch fin thickness fin height diffusion coefficient particle size cycle time cycle ratio temperature of hot water fluid velocity porosity	• SCP COP	Asynchronous
[25]	• Desorption temperature Cycle time Heat and mass recovery time	• SCP COP	Simultaneous
[26]	• Fin spacing	• Sorbent temperature difference Adsorber bed/adsorbent mass	Simultaneous
[27]	• Cycle time	• VSCP COP	Asynchronous
[28]	• Cooling time mass recovery time heat recovery time	• SCP COP	Asynchronous
[29]	• Cycle time	• SCP COP	Asynchronous
[30]	• Mass recovery time switch time cycle time	• COP SCP	Asynchronous
[31]	• Fin height fin spacing	• COP SCP	Asynchronous
[32]	• Cycle time Adsorption/desorption time	• COP SCP	Asynchronous
[33]	• Adsorption time Desorption time Particle diameter Number of fins	• COP SCP	Simultaneous
[34]	• Cycle time mass recovery time preheating and precooling time	• SCP COP	Asynchronous
[35]	• Fin spacing	• SCP COP TCP	Asynchronous
[36]	• Adsorption time desorption time	• COP TCP	Simultaneous
[37]	• Desorption/adsorption time fin height fin number	• SCP COP	Asynchronous

Table 2
A summary of the available studies with a reasonable compromise between SCP and COP.

Ref.	Sorption pair	S-HMX	τ (min)	Q_{evap} (kW)	SCP (W/kg)	COP
[41]	Coating silica gel + $CaCl_2$(SWS-1l)/water	Aluminum finned tube	10	0.48	137	0.15
[42]	Coating AQSOA-FAM-Z02/water	Extruded aluminum finned-tube heat exchanger	–	0.442	295	0.21
[43]	Silica gel/water	Aluminum finned tube	6	1.9	158	0.29
[44]	Loose grain $LiNO_3$–Silica KSK/water (SWS-9l)	Aluminum finned flat tube	6.4		318	0.176
[20]	Loose grain AQSOA-FAM Z02/water	Aluminum finned flat tube	7	0.155	394	0.6
[45]	Coating zeolite, SAPO-34/water	Aluminum finned flat tube	5		675	0.24
[46]	Coating SAPO-34/water	Aluminum sintered metal fiber structures soldered on flat fluid channels	10	5	852	0.4
[47]	Coating AQSOA-FAM-Z02/water	Finned tube (copper)	1.5	1.5	872	0.27
[48]	Coating silica gel + $CaCl_2$/water	Aluminum finned-copper tube engine oil cooler	10	0.306	235	0.2

$$SCP = \frac{Q_{evap}}{m_{sorb}\tau} = \frac{m_{sorb}\int_{ads}\frac{d\omega}{dt}h_{fg}dt}{m_{sorb}\tau} = \frac{\Delta\omega\, h_{fg@T_{evap}}}{\tau} \quad (1)$$

where, Q_{evap} is the evaporative cooling energy (J), m_{sorb} is the sorbent mass (kg), τ is the cycle time (s), h_{fg} is the sorbate enthalpy of evaporation (J/kg), and ω is the sorbate uptake (g sorbate/g sorbent).

The coefficient of performance (COP) is defined as the ratio of evaporative cooling energy to the input energy, Eq. (2). The COP can be increased by: i) enhancing the heat and mass transfer processes inside S-HMX, which increases both the evaporative cooling energy and the desorption heat, which overall increases the COP; and ii) decreasing the sensible energy required to overcome the thermal inertia of the heat exchanger (HEX), sorbent material, refrigerant inside the sorbent and the heat transfer fluid.

$$COP = \frac{Q_{evap}}{Q_{input}} = \frac{Q_{evap}}{Q_{sens} + Q_{des}} = \frac{m_{sorb}\int_{ads}\frac{d\omega}{dt}h_{fg}dt}{\int_{des}\left(\left(m_{HEX}c_{p,HEX} + m_{sorb}\left(c_{p,s} + \omega c_{p,w}\right)\right)\frac{dT}{dt} - m_{sorb}\frac{d\omega}{dt}h_{ads}\right)dt} \quad (2)$$

where, Q_{evap} is the evaporative cooling energy (J), Q_{input} is the input thermal energy (J), Q_{sens} is the thermal energy required to overcome thermal inertia of the sorber bed heat and mass exchanger (J), Q_{des} is the thermal energy consumed for desorption (J), m_{sorb} is the sorbent mass (kg), m_{HEX} is the heat exchanger (HEX) mass (kg), h_{fg} is the sorbate enthalpy of evaporation (J/kg), c_p is the specific heat (J/(kg K)), ω is the sorbate uptake (g sorbate/g sorbent), T is the sorbent temperature (K), and h_{fg} is the sorbate enthalpy of sorption (J/kg).

Table 3
Three levels of S-HMX design parameters.

	Level 1	Level 2 (baseline case)	Level 3
Fin height (b (cm))	1	2	3
Fin thickness (t_f (mm))	1	2	3
Sorbent thickness (t_s (mm))	1	2	3
Graphite flake content in sorbent (ϕ (wt. %))	0	10	20
Cycle time (τ (min))	10	15	20
Fluid tube radius (r_1), fluid channel height ($H_c/2$ (mm))	2	3	4

3. Analysis of variance (ANOVA)

Analysis of variance (ANOVA) is a systematic method that can be used to evaluate the impact of design parameters on the performance by calculating the sums of square, level of contribution, F-statistic ratio and p-value, see Ref. [49–51] and Appendix C for more details. In this study, the effect of S-HMX design parameters on the SCP and COP is investigated using ANOVA in MATLAB and the 2-D analytical model developed in our previous study for the P-HMX [48]. Also, a new 2-D analytical model has been developed for the F-HMX in cylindrical coordinate, described in Appendix A. A Box–Behnken design [52] with three levels of design parameters shown in Table 3 is used to generate the sample points. The design parameters used in Table 3 are shown in Fig. A1 and Fig. A2 in Appendix A. It should be noted that the effect of graphite flake content on the thermophysical properties and water uptake of the composite sorbent was studied in Ref. [40] and implemented in this paper.

Fig. 1 shows the level of contribution of each design parameter to the SCP and COP for the two targeted sorber beds, the P-HMX and F-HMX. The following can be concluded:

- The sorbent thickness and cycle time have the highest level of contribution to the SCP.
- The fin thickness, fin height and the amount of graphite flake (thermally-conductive additive) in the sorbent have the second largest level of contribution to SCP.

Table 4
p-value of design parameters to the SCP and COP of the P-HMX and F-HMX.

	P-HMX		F-HMX	
	SCP	COP	SCP	COP
b	5.85e-6	6.66e-16	1.78E-15	7.77e-16
t_f	1.61e-8	8.14e-36	8.72E-13	3.19e-27
t_s	7.05e-28	2.76e-28	4.16E-26	1.39e-28
ϕ	4.41e-11	6.66e-16	2.48E-7	2.86e-8
τ	5.64e-34	2.58e-21	9.04E-36	3.33e-16
r_1, $H_c/2$	1.22e-2	1.03e-2	1.03E-2	2.75e-3

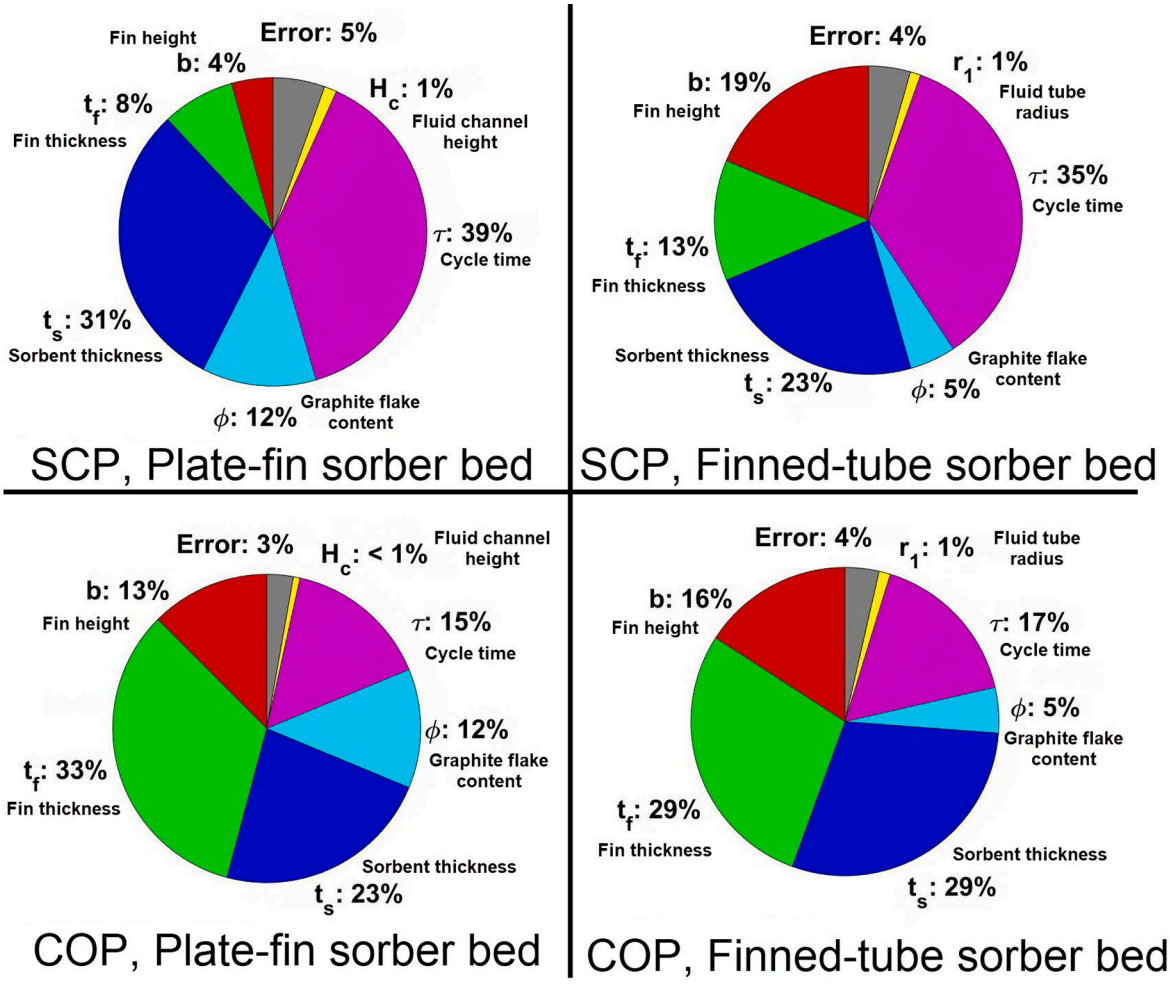

Fig. 1. The level of contribution of design parameters to the SCP and COP of the P-HMX and F-HMX, b: fin height, t_f: fin thickness, t_s: sorbent thickness, ϕ: graphite flake content in sorbent, τ: cycle time, H_C: fluid channel height in the P-HMX, and, r_1: fluid tube radius in the F-HMX, The design parameters are shown in Fig. A1 and Fig. A2 in Appendix A. More information on the level of contribution and the error is presented in Appendix C.

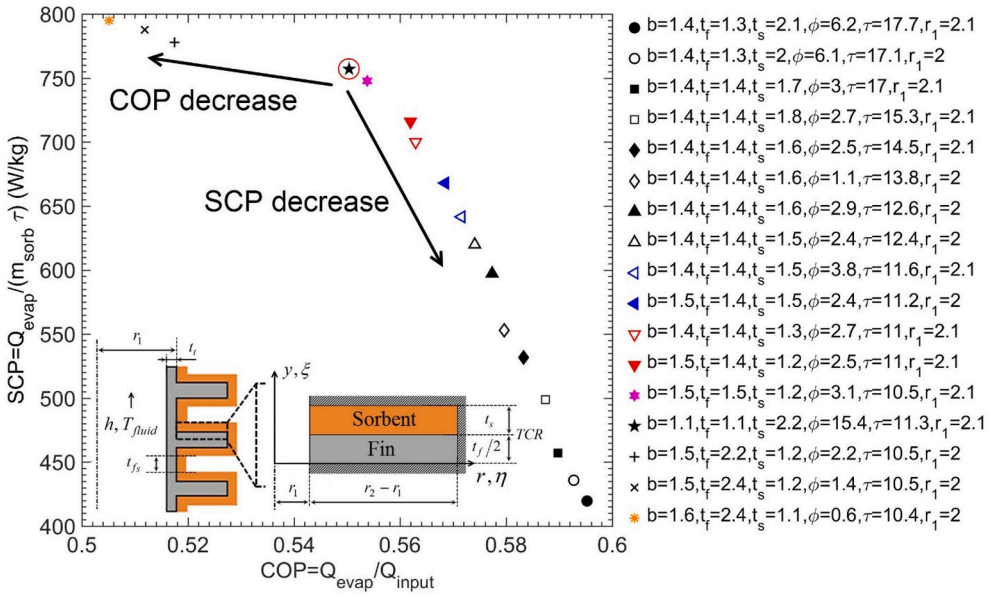

Fig. 2. The set of optimum solutions for the F-HMX, trade-off between the SCP and COP, b: fin height (r_2-r_1) (cm), t_f: fin thickness (mm), t_s: sorbent thickness (mm), ϕ: graphite flake content in sorbent (wt.%), τ: cycle time (min), r_1: fluid tube radius (mm), see Fig. A2 in Appendix A for a schematic of the S-HMX and parameters.

- The heat transfer fluid (HTF) channel height and tube radius have the lowest level of contribution to SCP.
- Fin thickness and sorbent thickness have the largest impact on COP.
- Cycle time, fin height and the amount of graphite flake in the sorbent have a relatively lower effect on COP.
- The HTF channel height and fluid tube radius have the lowest impact on COP.

Table 4 presents the p-value of each design parameter for the SCP and COP of the P-HMX and F-HMX. It can be seen that all of the design parameters have significant contribution to the SCP and COP because all the p-values are lower than a 0.05 level of significance. Hence, the entire S-HMX, consisting of the sorbent, heat exchanger and the heat transfer fluid, should be optimized simultaneously to achieve an optimal set of the SCP and COP.

4. Optimization study

As mentioned in Section 0, the sorber bed geometry, heat transfer characteristics and cycle time should be optimized simultaneously. Hence, using the 2-D analytical model and a multi-objective genetic algorithm, the geometry and heat transfer characteristics of both the P-HMX and F-HMX are determined to optimize the SCP and COP. The constraints are defined based on the parametric study in Ref. [6], and the ANOVA in Section 3. The variables are: i) fin height 1–3 cm; ii) fin thickness 0.5–3 mm; iii) sorbent thickness 1–3 mm; iv) graphite flake content 0–20 wt%; v) cycle time 10–20 min; and vi) fluid channel height 4–8 mm or radius 2–4 mm. The multi-objective optimization problem can be represented as follows [53].

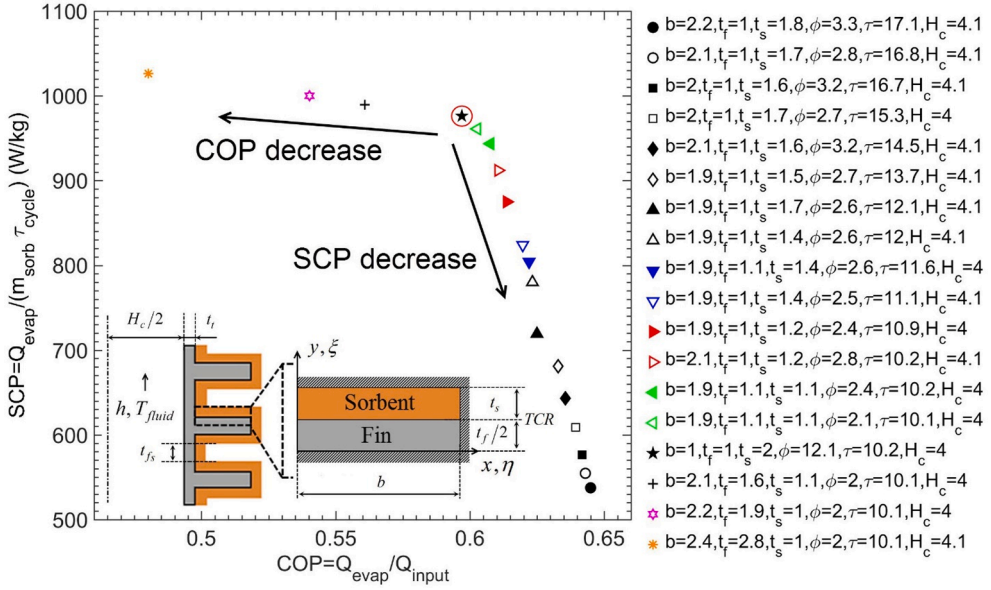

Fig. 3. A set of optimum solutions for the P-HMX, trade-off between the SCP and COP, b: fin height (cm), t_f: fin thickness (mm), t_s: sorbent thickness (mm), ϕ: graphite flake content in sorbent (wt.%), τ: cycle time (min), H_C: fluid channel height (mm), see Fig. A1 in Appendix A for a schematic of the S-HMX and parameters.

Table 5
Specifications of the P-HMX and F-HMX.

Characteristics	P-HMX	F-HMX
Fin height (cm)	1	1.1
Fin thickness (mm)	1	1.1
Fin spacing (mm)	4	4.4
Fluid channel height/fluid tube diameter (mm)	4	4
Fluid channel width (cm)	1.27	–
Total length without the tubes (cm)	31	32
Total width (cm)	20	20
Tube outer diameter (cm)	1.9	1.9
Tube length (cm)	12	12
Volume of the S-HMX without the tubes outside the vacuum chamber (L)	1.7	2.05
Volume of the S-HMX filled with sorbent (L)	0.974	0.655
Heat transfer surface area between the sorbent and the heat exchanger (m^2)	0.577	0.327
Mass of the heat exchanger without sorbent coating and tubes outside the vacuum chamber (kg)	1.72	1.04
Mass of sorbent coating (kg)	0.587	0.379
Mass of heat transfer fluid (water) (kg)	0.498	0.123
Ratio of sorbent mass to the heat exchanger mass (m_{sorb}/m_{HEX})	0.34	0.36
Mass percentage of silica gel B150	39	37.5
Mass percentage of $CaCl_2$	39	37.5
Mass percentage of PVA	10	10
Mass percentage of graphite flakes	12	15

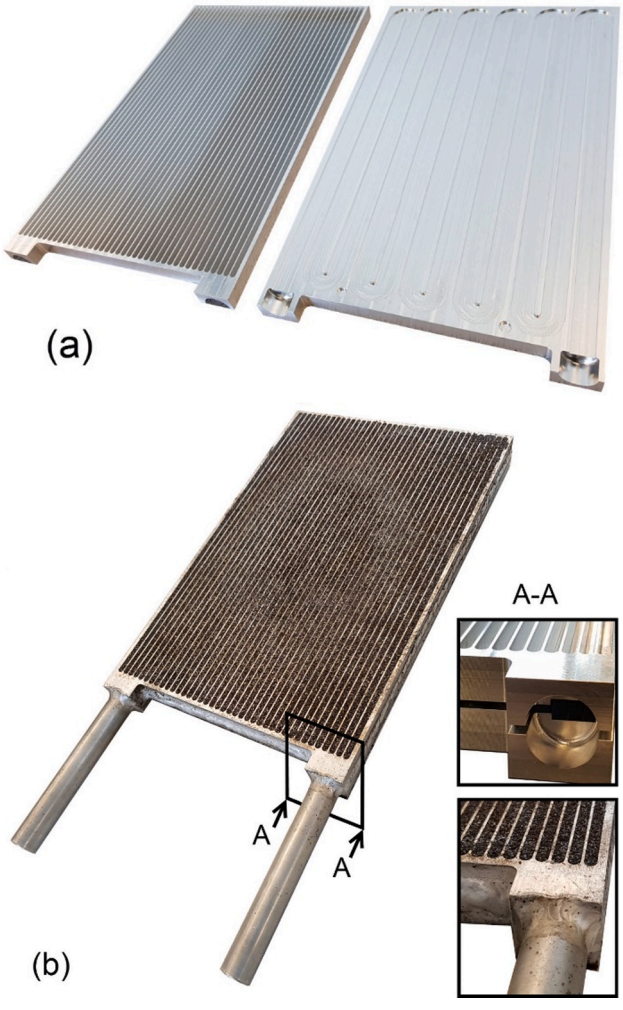

Fig. 4. (a) Two halves of the P-HMX showing the fin side and the fluid channel side; and (b) an assembled P-HMX coated with the composite sorbent, silica gel, $CaCl_2$, PVA and graphite flakes.

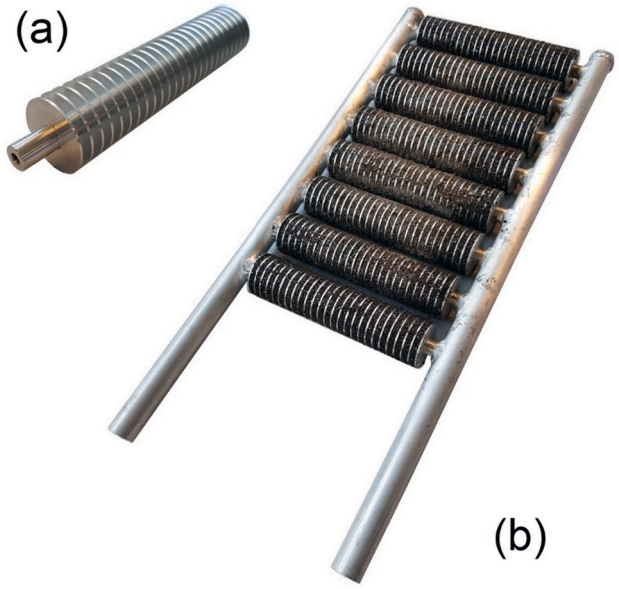

Fig. 5. (a) One aluminum finned-tube; and (b) an assembled F-HMX coated with the composite sorbent, silica gel, $CaCl_2$, PVA and graphite flakes.

$$\min_{\text{wrt } \vec{x}} \ [-\text{SCP}, \ -\text{COP}] \qquad \vec{x} = [b, t_f, t_s, \phi, \tau, H_c] \tag{3}$$

Using the multi-objective genetic algorithm in MATLAB, 15,401 times for the P-HMX, Cartesian analytical model; and 16,451 times for the F-HMX, cylindrical analytical model, were used to evaluate the SCP and COP. Function tolerance and crossover fraction were set to 1e-6 and 0.8, respectively. The sets of optimum solutions for the F-HMX and P-HMX, i.e. the trade-off between the SCP and COP, are presented in Fig. 2 and Fig. 3, respectively. The design that can achieve SCP of 757 W/kg and COP of 0.55 is selected for F-HMX, and the design with the SCP of 976 W/kg and COP of 0.60 is selected for P-HMX, due to an optimal compromise between SCP and COP. P-HMX and F-HMX optimum design is built and tested, which is discussed in the following sections. It should be noted that all the design points in Fig. 2 and Fig. 3 are optimum and they could be selected based on the application. For example, points with higher COP could be selected for applications with a limited amount of heat source, while points with higher SCP could be chosen if the system mass is the main constraint. Moreover, the same ANOVA and optimization study can be conducted for different sorption systems by changing the operating conditions and the objective functions, such as thermal energy storage capacity, specific heating power, moisture removal capacity, etc.

5. Characteristics of P-HMX and F-HMX

Two sorber bed heat and mass exchangers of the P-HMX and F-HMX were built based on the optimization study in Section 4. The specifications of the P-HMX and F-HMX are presented in Table 5. Fig. 4 (a) shows two halves of the P-HMX with fin side and fluid channel side. The spacing between the fins, the serpentine HTF channels and the half-circle regions for the aluminum tube were machined out of two aluminum 6061 plates using our CNC milling machine. Moreover, male and female connections were machined on the plates for alignment. After that, two halves of the P-HMX and two aluminum tubes were welded together. Building the P-HMX by extrusion can reduce the manufacturing cost significantly, but it increases the capital cost due to the die required; hence, it may be more suitable for mass production.

Fig. 5 (a) shows the aluminum finned-tubes fabricated to manufacture the F-HMX. The aluminum finned-tubes were built using our CNC

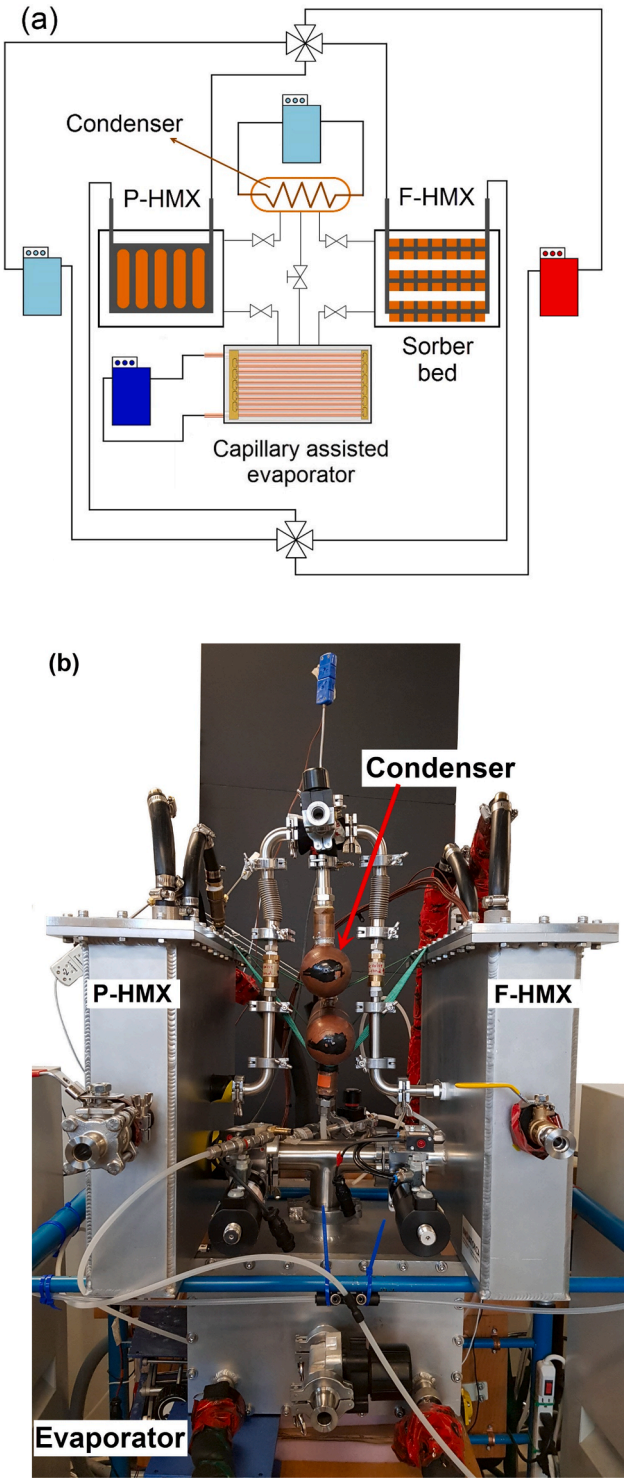

Fig. 6. (a) A schematic; and (b) a picture of two-sorber bed sorption test bed, capillary-assisted evaporator in the chamber at the bottom, P-HMX and F-HMX in the chambers on the sides, two helical coil and shell heat exchangers as condenser at the top.

lathe machine, and welded to an aluminum tube as a header. Two plugs were machined and welded to the ends of the aluminum tube header. The diameter of the finned-tubes is 4 mm, and the tube header diameter is 13 mm; thus, the pressure drop in the finned-tubes is two orders of magnitude larger than that of the tube header; consequently, the fluid flow in the eight finned-tubes can be assumed uniformly distributed.

Polyvinyl alcohol (PVA) binder (Sigma-Aldrich) was dissolved in distilled water. Subsequently, $CaCl_2$ and silica gel (SiliaFlash® B150, Silicycle, Inc., Quebec, Canada, with diameter of 250–500 μm and average pore size of 15 nm) and graphite flakes (consisting of both 150 μm fine particles and thin flakes up to 1.3 mm long, Sigma-Aldrich) were added to the aqueous solution. More information about the composite sorbents and their selection can be found in Ref. [40]. Subsequently, the solution was heated on a hot plate until most of the water was evaporated and the solution became viscous. Afterwards, the fin spacings of the P-HMX and F-HMX were filled with the slurry solution of the optimum composite sorbent shown in Table 5. Finally, the composite sorbent was dried at 80 °C and then cured at 180 °C in the oven. Fig. 4 (b) and Fig. 5 (b) show the assembled P-HMX and F-HMX coated with the optimum composite sorbent.

6. Experimental study

Fig. 6 shows the schematic and the picture of two-sorber bed sorption test bed custom-built to test the P-HMX and F-HMX side-by-side. The P-HMX and F-HMX were placed inside aluminum vacuum chambers on the sides, a custom-designed capillary-assisted evaporator was positioned in the bottom aluminum vacuum chamber, and two helical coil and shell heat exchangers were used as a condenser at the top. Check valves were installed between the S-HMXs and the condenser and gate valves were installed between the evaporator and the S-HMXs. A needle valve with high precision flow adjustment (Speedivalve SP16K, Edwards) and a U-tube were installed between the condenser and the evaporator. The test bed was vacuumed for 6 h before the tests. Two temperature control systems were used to keep the evaporator at 15 °C and the condenser at 30 °C to mimic the cooling zone and the ambient, respectively. Furthermore, two temperature control systems were set to 90 °C and 30 °C for desorption and sorption processes, to mimic the heat source and the ambient, respectively. Two four-way valves were employed to switch the heat transfer fluid between two S-HMXs for desorption and sorption processes. One of the four-way valves was set to have a delay at the beginning of each process to push the high- and low-temperature heat transfer fluid in S-HMXs and hoses back to high- and low-temperature reservoirs of temperature control systems to perform a heat recovery process. The time delay was calculated as 10 s based on the flow rate of the heat transfer fluid and the fluid volume in the sorber beds and the hoses. The resistance temperature detector (RTD) (PT100) temperature sensors (Omega, model #PR-13–2-100–1/8–6-E) with an accuracy of 0.15 °C and pressure transducers with a 0–34.5 kPa operating range (Omega, model #PX309-005AI) and 0.4 kPa accuracy were installed to monitor and record the temperature and pressure variations in each component of the sorption test bed over time. Positive displacement flow meters (FLOMEC, Model # OM015S001-222) with an accuracy of 0.5% of reading were installed to measure the flow rate of the heat transfer fluid of the condenser, evaporator and the cooling circuit of the S-HMX. Since the positive displacement flow meters may impede the flow at higher temperatures, ultrasonic flowmeter (Kobold model DUK-1xx6) with accuracy of 0.7% of reading was used to measure the flow rate of the high-temperature heat transfer fluid to the S-HMXs. The instruments were interfaced with a PC through a data acquisition system and in-house software built in the LabVIEW environment. Experiments were performed continuously until the system reached an oscillatory steady state. The maximum uncertainties in the calculations of the SCP and COP were calculated to be 10.6% and 12.5%, respectively. More information on the custom-designed capillary-assisted evaporator can be found in Ref. [54]. More information on uncertainty analysis is presented in Appendix B.

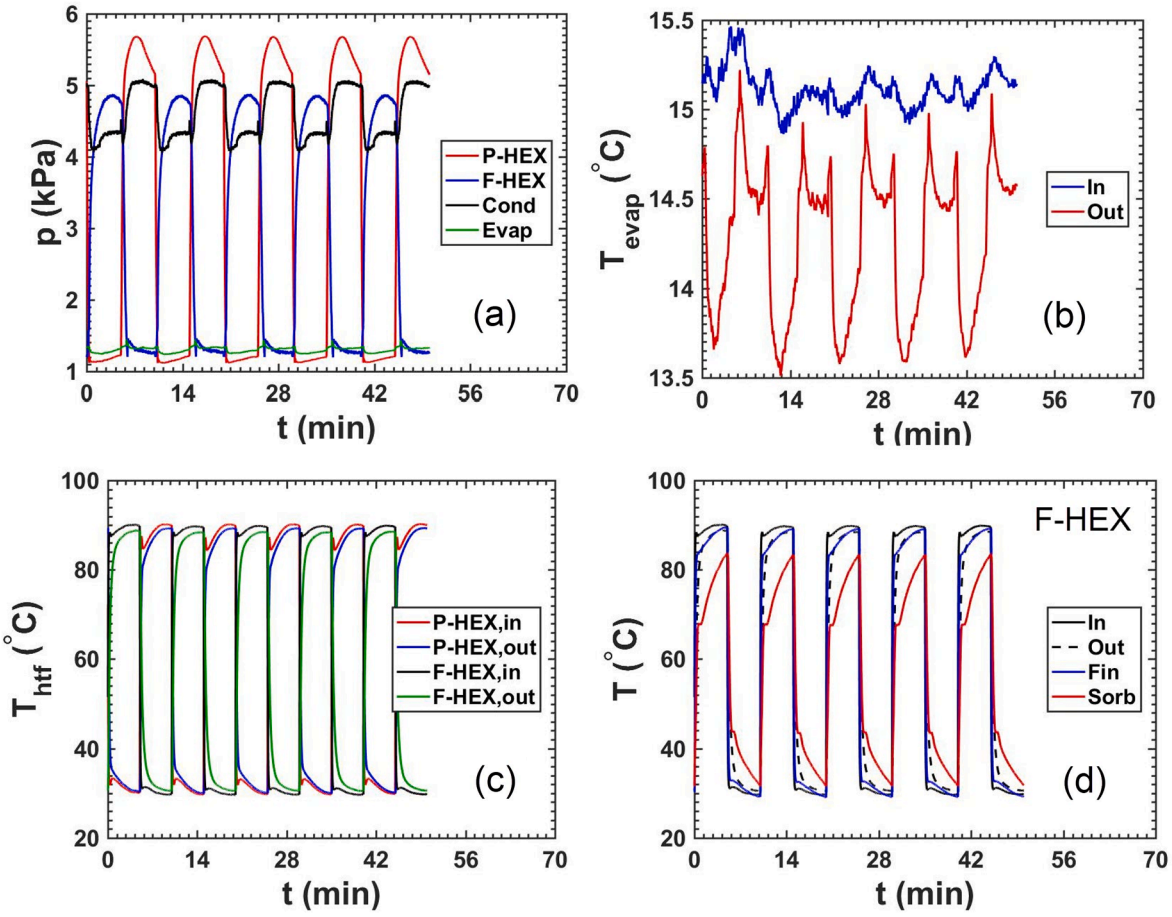

Fig. 7. Temporal variation of: (a) pressure of the P-HMX, F-HMX, condenser and evaporator; (b) inlet and outlet temperatures of the HTF to evaporator; (c) inlet and outlet temperatures of the HTF to the P-HMX and F-HMX; and (d) temperatures of inlet and outlet HTF, fin and sorbent in the F-HMX, for $T_{des} = 90$ °C, $T_{amb} = 30$ °C, $T_{evap} = 15$ °C and $\tau_{cycle} = 10$ min; the HTF: heat transfer fluid.

7. Results and discussion

Fig. 7 shows the temporal variation of: (a) pressure of the P-HMX, F-HMX, condenser and evaporator; (b) inlet and outlet temperatures of the HTF to evaporator; (c) inlet and outlet temperatures of the HTF to the P-HMX and F-HMX; and (d) the temperatures of inlet and outlet HTF, fin and sorbent in the F-HMX, for $T_{des} = 90$ °C, $T_{sorp} = T_{cond} = 30$ °C, $T_{evap} = 15$ °C and $\tau_{cycle} = 10$ min. The following can be concluded from Fig. 7:

- The sorber bed pressures are higher than that of the condenser during desorption and lower than that of the evaporator during the sorption to cause condensation and evaporation, respectively. The P-HMX can cause higher pressure levels during desorption and lower pressure during sorption due to: (i) higher performance of the P-HMX; and (ii) more sorbent material of the P-HMX compared to the F-HMX (0.587 kg vs 0.379 kg). However, after the desorption process with each sorber bed, the condenser pressure approaches 4.2 kPa, which is the saturation pressure at 30 °C.
- The temperature difference between the inlet and outlet HTF of the evaporator in Fig. 7 (b) indicates the cooling power generated by the P-HMX and F-HMX. The half-cycles with minimum temperature about 13.5 °C correspond to the P-HMX. The reasons for higher cooling power provided by the P-HMX are: (i) higher performance of the P-HMX; and (ii) more sorbent material of the P-HMX compared to the F-HMX (0.587 kg vs 0.379 kg).
- Fig. 7 (c) shows that the temperature differences between the inlet and outlet HTF to the P-HMX is smaller than the F-HMX because the flow rate is higher when the temperature control systems (TCS) are connected to the P-HMX compared to the F-HMX due to higher pressure drop of the F-HMX. For example, the flow rates of the P-HMX and F-HMX are 11.45 l/min and 4.23 l/min during desorption, respectively. Based on the experiments and the analytical models, the performance of the P-HMX and F-HMX does not change significantly for flow rates higher than 2 l/min because the HTF thermal resistance is not the controlling component.
- Fig. 7 (d) shows that the average fin temperature of the F-HMX is close to the HTF outlet temperature. Moreover, the average sorbent temperature has a bump with a delay after the beginning of each sorption and desorption process. After this point, there is a higher temperature difference between the sorbent and the fin. The reason is that due to the thermal inertia of the S-HMX, there is a delay in the time when the sorbent temperature is high enough for desorption and low enough for sorption. This delay can be observed in Fig. 7 (a) when the S-HMX pressure is almost equal to that of evaporator and condenser, and the sorption and desorption processes begin. It takes the sorber beds a specific time (in this case about 25 s) to reach the evaporator and condenser pressure to start the sorption and desorption due to thermal inertia. We open the valves when that happens, otherwise the beds would desorb to the evaporator instead of adsorbing.

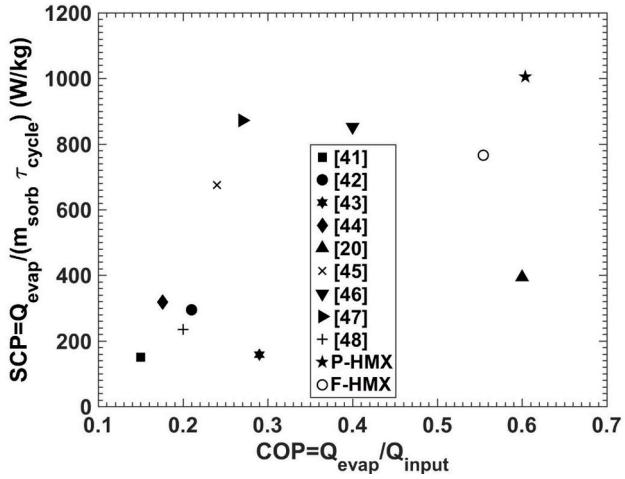

Fig. 8. Comparison of the P-HMX and F-HMX versus the available studies in Table 2 in terms of the SCP and COP.

7.1. Performance evaluation of P-HMX and F-HMX

The baseline case for the operating conditions of sorption air-conditioning is considered as the following: T_{des} = 90 °C, T_{sorp} = T_{cond} = 30 °C, T_{evap} = 15 °C, and τ_{cycle} = 10 min. Performance parameters of the SCP and COP are calculated based on Eqs. (1) and (2). For the baseline case, the P-HMX achieves a SCP of 1,005 W/kg sorbent and a COP of 0.60, whereas the F-HMX yields a SCP of 766 W/kg and a COP of 0.55. Fig. 8 shows the performance of the P-HMX and F-HMX versus the previously published studies in Table 2. It can be seen that the P-HMX provides the highest SCP and COP using the composite silica gel/$CaCl_2$ sorbent whose sorption occurs over the entire range of relative pressure $0.06 < p/p_0 < 0.4$, suitable for AC application [40]. On the other hand, zeolite-based sorbents, such as SAPO-34 and AQSOA FAM Z02, were used in Ref. [13,42,38–40], whose sorption takes place in a narrow range of p/p_0, which limits the application to relatively high desorption temperature, i.e. heat source of 80–90 °C, and low condenser temperature, i.e. temperature about 30 °C. It can be seen that the P-HMX provides 4.3 times higher SCP, and 3 times higher COP compared to an off-the-shelf heat exchanger, an engine oil cooler coated with a composite sorbent consisting of $CaCl_2$, silica gel B150 and PVA, presented in Ref. [48]. It clearly demonstrates the potential of specific design and optimization of the S-HMX for the SCS.

7.2. Effect of operating conditions

To investigate the effect of operating conditions on the P-HMX and F-HMX, the baseline case of T_{des} = 90 °C, T_{sorp} = T_{cond} = 30 °C, T_{evap} = 15 °C and τ_{cycle} = 10 min was selected and one parameter was varied while the others were kept constant. Fig. 9 shows the variation of the SCP and COP of the P-HMX and F-HMX with cycle time and the desorption, sorption, condenser and evaporator temperatures. A good agreement between the developed 2-D analytical model [48] and the experimental results can be seen, with an average and maximum relative differences of 3% and 7%, respectively. The following can be concluded from Fig. 9:

- As expected, by decreasing the cycle time, SCP increases as the sorption rate is higher at the beginning of sorption and reduces as the sorbent approaches saturation. Also, by decreasing the cycle time, the COP reduces because the heat required to overcome the S-HMX thermal inertia increases compared to the heat needed for desorption.
- By increasing the desorption temperature, the SCP increases because the differential water uptake between sorption and desorption increases as indicated in Fig. 10 (a). By increasing the desorption temperature, the COP increases and then decreases; thus, there is an optimum desorption temperature corresponding to maximum COP. The reason is the conflicting effects of increasing the SCP and increasing the sensible energy required to overcome the S-HMX thermal inertia due to higher temperature difference between desorption and sorption, by increasing the desorption temperature.
- By increasing the sorption and condenser temperature, the SCP reduces as the differential water uptake between sorption and desorption decreases as shown in Fig. 10 (b). Furthermore, by increasing the sorption and condenser temperature, the COP remains almost constant. The reason is the counteracting effects of decreasing the SCP and decreasing the sensible energy required to overcome the S-HMX thermal inertia due to a lower temperature difference between desorption and sorption, by increasing the sorption temperature.
- By increasing the evaporator temperature, both the SCP and COP increase because of higher differential water uptake between sorption and desorption as shown in Fig. 10 (c).

8. Conclusion

The analytical design tool developed in our previous work for sorber bed heat and mass exchangers (S-HMX) with plate fin heat and mass exchanger (P-HMX) in Cartesian coordinate, was applied and extended to a finned-tube heat and mass exchanger (F-HMX) in cylindrical coordinate system. The level of contribution of the S-HMX design parameters to the SCP and COP showed that the entire S-HMX, consisting of the sorbent, heat exchanger and the heat transfer fluid should be optimized simultaneously to achieve an optimal SCP and COP. To this end, a multi-objective optimization study was performed; a design with an SCP of 976 W/kg and a COP of 0.60 for the P-HMX, and a design with an SCP of 757 W/kg and a COP of 0.55 was selected for the F-HMX. The two new S-HMX designs were built based on the optimization study on the characteristics of the S-HMXs, consisting of the sorbent, heat exchanger and heat transfer fluid, namely: i) fin thickness; ii) fin height; iii) sorbent thickness; iv) fluid channel height; v) the amount of thermally-conductive additive in the sorbent; and vi) cycle time. It was shown that compared to the state-of-the-art, the new P-HMX provided the highest SCP, i.e. 1,005 W/kg sorbent, and the highest COP of 0.60. The results showed that by using the proposed optimization approach of the S-HMX, the performance could be increased significantly, i.e. 4.3 times higher SCP, and 3 times higher COP, compared to an off-the-shelf S-HMX, an engine oil cooler. The present P-HMX was tested under various operating conditions: i) desorption temperature, 60 to 90 °C; ii) sorption and condenser temperature (20–40 °C); iii) evaporator temperature (5–20 °C); and iv) cycle time (10–20 min). A SCP in the range of 320–1230 W/kg and a COP of 0.40–0.80 were measured in our test bed over the range of targeted operating conditions.

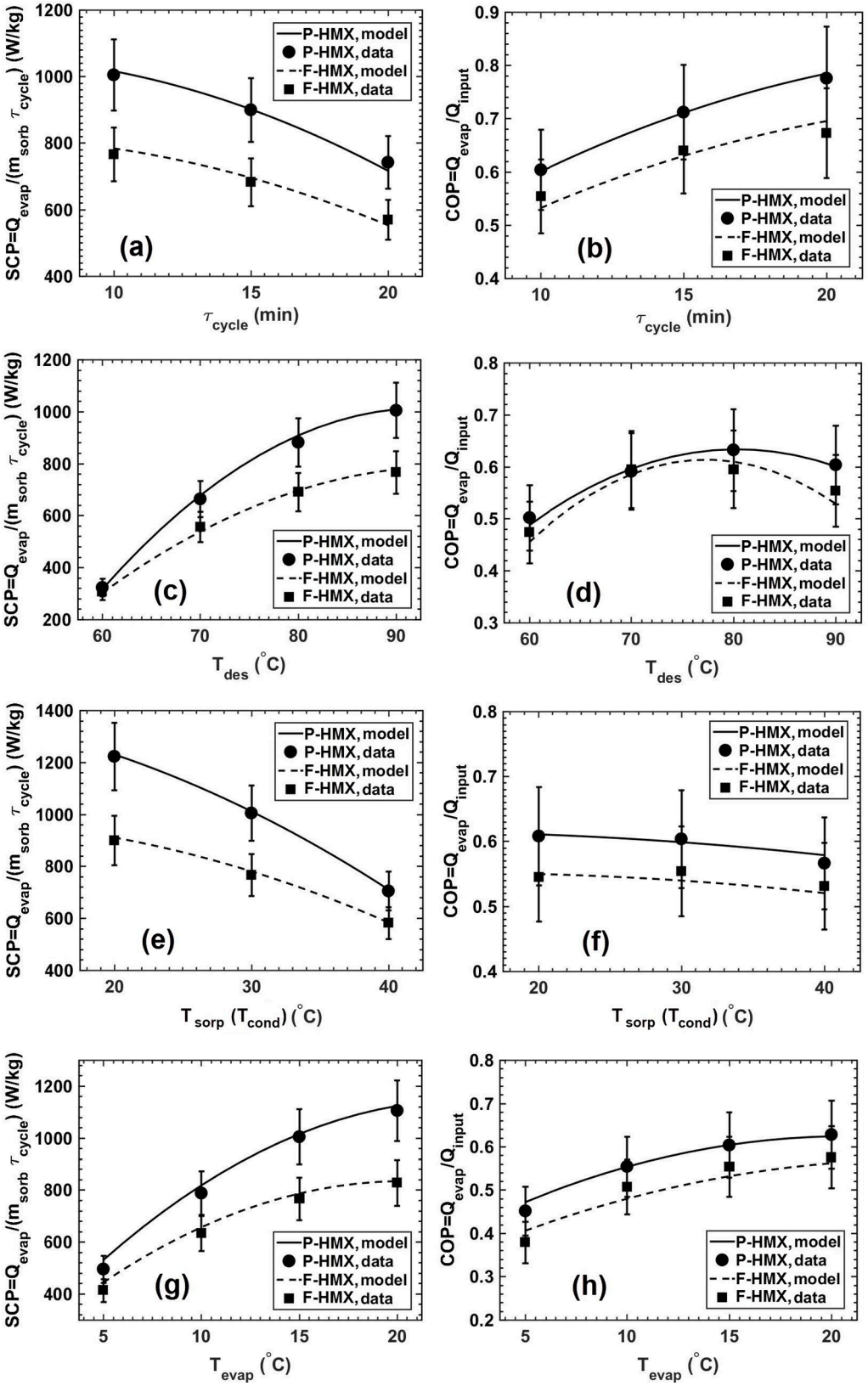

Fig. 9. Variation of SCP and COP of P-HMX and F-HMX with cycle time and temperatures of desorption, sorption, condenser and evaporator.

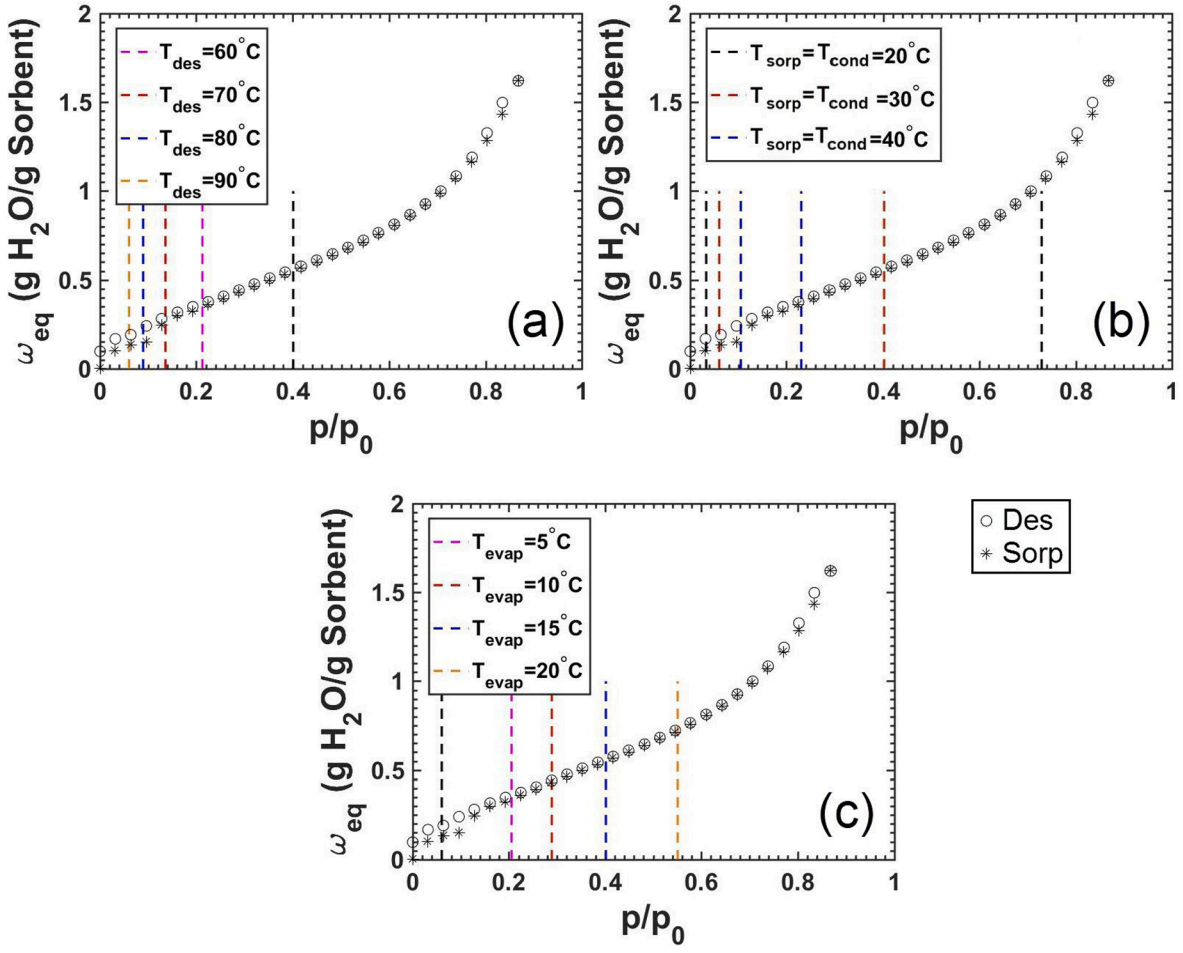

Fig. 10. The range of differential water uptake and p/p_0 for different temperatures of desorption, sorption and condenser and evaporator, isotherm plots are for composite sorbents with 39 wt% silica gel B150, 39 wt% $CaCl_2$, 10 wt% PVA binder and 12 wt% graphite flakes [40]

Declaration of Competing Interest

The authors declared that there is no conflict of interest.

Acknowledgement

The authors would like to thank Mr. G. Mustafa Sajid and Mr. James Shoults at Simon Fraser University's machine shop for their help with manufacturing the optimized sorber bed heat and mass exchangers. The authors gratefully acknowledge the financial support of the Natural Sciences and Engineering Research Council of Canada (NSERC) through the Idea to Innovation (I2I) Grant No. I2IPJ 530368-2018.

Appendix A. . Model development

A 2-D analytical model was developed in Cartesian coordinate for the P-HMX in our previous study [48], the solution domain is shown in Fig. A1.

In this section, a similar analytical model is developed in cylindrical coordinate system for the F-HMX. The solution domain of the F-HMX, shown in Fig. A2, can be used to predict the performance of the entire S-HMX. The assumptions in the model development are exactly the same as those of Ref. [48]:

- The heat transfer fluid is assumed to have a constant temperature along the solution domain;
- The boundaries of the sorbent and the fin, which are in contact with low-pressure refrigerant vapor, are assumed adiabatic;
- The thermophysical properties of the sorbent and the HEX are assumed constant. Averaged values over the range of operating conditions are used;
- The convection term in the energy equation, which accounts for the sorbate convection inside the sorbent coating, is assumed negligible; and
- The sorbent coated on the tube in the gap between the sorbent coatings on the fins, i.e. t_{fs} shown in Fig. 1, is neglected as t_{fs} is much smaller than the fin height.

The justification of the assumptions are presented in Ref. [48].

The energy equation for the sorbent layer and the fin in cylindrical coordinates can be written as follows.

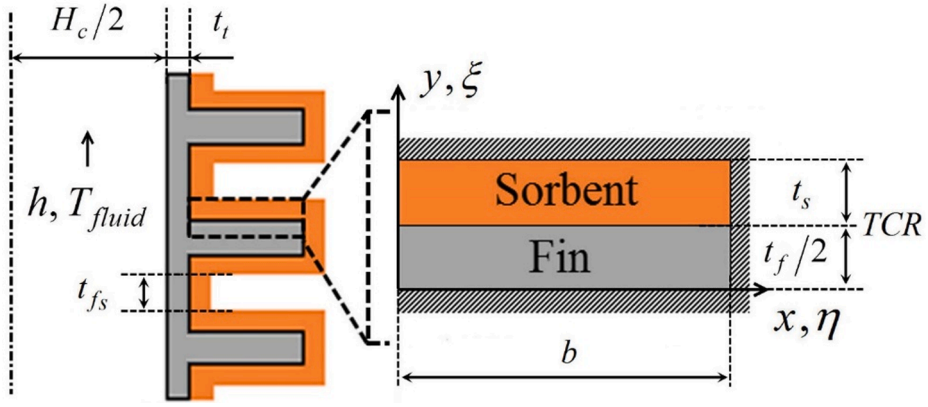

Fig. A1. Solution domain used in the 2-D analytical model for plate-fin heat exchanger in Cartesian coordinate system [48]

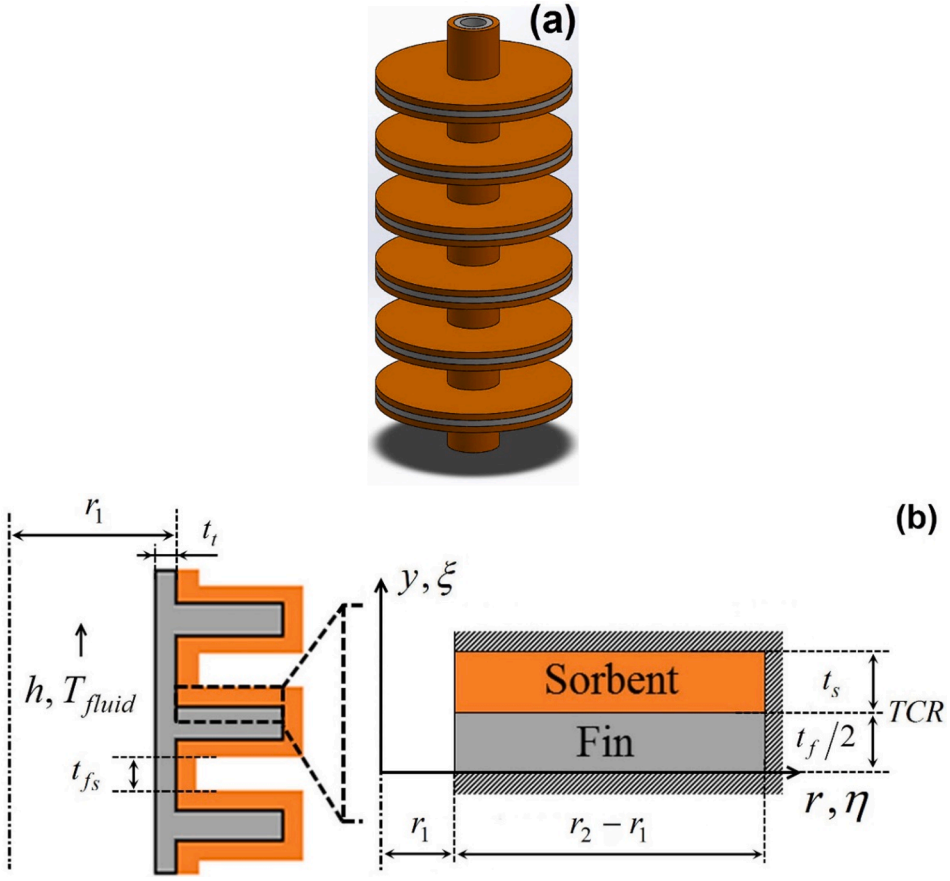

Fig. A2. (a) A 3D schematic; and (b) the solution domain for a finned-tube heat and mass exchanger (F-HMX).

$$\frac{\partial T_i}{\partial t} = \alpha_{i,r}\left(\frac{\partial^2 T_i}{\partial r^2} + \frac{1}{r}\frac{\partial T_i}{\partial r}\right) + \alpha_{i,y}\frac{\partial^2 T_i}{\partial y^2} + \frac{1}{(\rho c_p)_i}G_i(t) \qquad T_i(r,y,t) \qquad i = s,f \tag{A1}$$

$$G_i(t) = \begin{cases} \rho_s h_{ads}\dfrac{d\omega}{dt}, & i = s \\ 0, & i = f \end{cases} \tag{A2}$$

where, i = s, f represents the sorbent and fin domains, respectively. The convective boundary conditions are:

$$\frac{1}{R_s}\left(T_s(r_1,y,t) - T_{fluid}\right) = k_s\frac{\partial T_s(r_1,y,t)}{\partial r} \tag{A3}$$

$$\frac{1}{R_f}\left(T_f(r_1,y,t)-T_{fluid}\right)=k_{f,r}\frac{\partial T_f(r_1,y,t)}{\partial r} \tag{A4}$$

$$R_s=2\pi r_1 t_s\left(\frac{ln(r_1/(r_1-t_t))}{2\pi k_{f,r}t_s}+\frac{1}{2\pi(r_1-t_t)t_s h}+TCR\right)\quad\left(\frac{K\,m^2}{W}\right) \tag{A5}$$

$$R_f=2\pi r_1 t_f\left(\frac{ln(r_1/(r_1-t_t))}{2\pi k_{f,r}t_f}+\frac{1}{2\pi(r_1-t_t)t_f h}\right)\quad\left(\frac{Km^2}{W}\right) \tag{A6}$$

where, the convective heat transfer coefficient is calculated by the correlation proposed by Gnielinski [55] as follows:

$$h=0.012\frac{k_w}{2r_1}\left(Re^{0.87}-280\right)Pr^{0.4} \tag{A7}$$

The adiabatic boundary conditions are:

$$\frac{\partial T(r_2,y,t)}{\partial r}=0 \tag{A8}$$

$$\frac{\partial T_s\left(r,t_s+t_f,t\right)}{\partial y}=0 \tag{A9}$$

Due to symmetry, one can write the following for the lower side of the fin:

$$\frac{\partial T_s\left(r,t_s+t_f,t\right)}{\partial y}=0 \tag{A10}$$

The continuity of heat flux, as well as the temperature jump/drop created by thermal contact resistance (TCR) are considered at the interface between the sorbent coating and fin as follows:

$$k_{f,y}\frac{\partial T_f\left(r,t_f,t\right)}{\partial y}=k_s\frac{\partial T_s\left(r,t_f,t\right)}{\partial y} \tag{A11}$$

$$-k_{f,y}\frac{\partial T_f\left(r,t_f,t\right)}{\partial y}=\frac{1}{TCR{\cdot}A}\left(T_f\left(r,t_f,t\right)-T_s\left(r,t_f,t\right)\right) \tag{A12}$$

The following non-dimensional variables can be defined.

$\theta=\frac{T-T_{fluid}}{T_0-T_{fluid}}$	$\xi=\frac{y}{t_s+t_f}$	$\eta=\frac{r}{r_2}$
$Bi_s=\frac{r_2}{R_s k_s}$	$Bi_f=\frac{r_2}{R_f k_f}$	$\kappa=\frac{k_s}{k_y}$
$\Lambda=\frac{t_s+t_f}{k_y TCR A}$	$Fo=\frac{t\alpha_r}{{r_2}^2}$	$\delta=\frac{r_2}{t_s+t_f}$
${\mu_y}^2=\frac{\alpha_y}{\alpha_r}$	${\mu_s}^2=\frac{\alpha_s}{\alpha_r}$	$\delta_f=\frac{t_f}{t_s+t_f}$
$\delta_r=\frac{r_1}{r_2}$		

where, θ is the dimensionless temperature, the Fourier number, Fo, is the dimensionless time, ξ and η are the dimensionless cylindrical coordinates. Using the aforementioned dimensionless variables, the dimensionless energy equation can be obtained as follows:

$$\frac{\partial\theta_i}{\partial Fo}={\mu_{i,\eta}}^2\left(\frac{\partial^2\theta_i}{\partial\eta^2}+\frac{1}{\eta}\frac{\partial\theta_i}{\partial\eta}\right)+\left(\mu_{i,\xi}\delta\right)^2\frac{\partial^2\theta_i}{\partial\xi^2}+g_i(Fo)$$
$$\theta_i(\eta,\xi,Fo) \tag{A13}$$
$$i=s,f$$

where

$$g_i(Fo)=\begin{cases}\dfrac{(1-\varepsilon)h_{ads}}{c_{p,s}\left(T_0-T_{fluid}\right)}\dfrac{d\omega}{dFo}, & i=s\\ 0, & i=f\end{cases} \tag{A14}$$

$$\mu_{i,\eta}=\begin{cases}1, & i=f\\ \mu_s, & i=s\end{cases} \tag{A15}$$

$$\mu_{i,\xi}=\begin{cases}\mu_y, & i=f\\ \mu_s, & i=s\end{cases} \tag{A16}$$

Water uptake can be modelled in terms of the operating conditions, i.e. pressure and temperature of the sorber bed. A linear relationship is obtained between the water uptake and sorbent temperature for each pressure during the isobaric sorption and desorption processes. Detailed explanation is presented in Ref. [48].

The dimensionless boundary conditions are:

$$\frac{\partial\theta_s(\delta_r,\xi,Fo)}{\partial\eta}-Bi_s\theta_s(\delta_r,\xi,Fo)=0 \tag{A17}$$

$$\frac{\partial\theta_f(\delta_r,\xi,Fo)}{\partial\eta}-Bi_f\theta_f(\delta_r,\xi,Fo)=0 \tag{A18}$$

$$\frac{\partial\theta_s(\eta,1,Fo)}{\partial\xi}=0 \tag{A19}$$

$$\frac{\partial\theta(1,\xi,Fo)}{\partial\eta}=0 \tag{A20}$$

$$\frac{\partial\theta_f(\eta,0,Fo)}{\partial\xi}=0 \tag{A21}$$

$$\frac{\partial\theta_f(\eta,\delta_f,Fo)}{\partial\xi}=\kappa\frac{\partial\theta_s(\eta,\delta_f,Fo)}{\partial\xi} \tag{A22}$$

$$-\frac{\partial\theta_f(\eta,\delta_f,Fo)}{\partial\xi}=\Lambda\left(\theta_f(\eta,\delta_f,Fo)-\theta_s(\eta,\delta_f,Fo)\right) \tag{A23}$$

The dimensionless energy equation, Eqs. (A13)–(A23), is solved using the Eigenfunction Expansion Method. The solution methodology is explained in Ref. [48] in detail. The difference between the present model, F-HMX, versus Ref. [48], the P-HMX, is the eigenvalue problem in η direction. In Cartesian coordinates, the eigenfunctions in η direction are sinusoidal, whereas in cylindrical coordinate, they are in the form of Bessel functions.

Based on Eqs. (A13)–(A23), the following eigen-value problem can be established in η direction.

$$\Phi''+\frac{1}{\eta}\Phi'+\gamma^2\Phi=0 \tag{A24}$$

$$\Phi'-Bi\,\Phi=0@\eta=\delta_r \tag{A25}$$

$$\Phi'=0@\eta=1 \tag{A26}$$

The following transcendental equation is obtained to evaluate the eigenvalues.

$$-\gamma J_1(\gamma\delta_r)+\frac{\gamma J_1(\gamma)}{Y_1(\gamma)}Y_1(\gamma\delta_r)-BiJ_0(\gamma\delta_r)+Bi\frac{J_1(\gamma)}{Y_1(\gamma)}Y_0(\gamma\delta_r)=0 \tag{A27}$$

The eigenfunction associated with each eigenvalue are given as follows:

$$\Phi=J_0(\gamma\eta)-\frac{J_1(\gamma)}{Y_1(\gamma)}Y_0(\gamma\eta) \tag{A28}$$

where, Bessel functions of the first and second kind are:

$$J_m(\eta)=\sum_{k=0}^{\infty}\frac{(-1)^k}{k!(k+m)!}\left(\frac{\eta}{2}\right)^{2k+m} \tag{A29}$$

$$Y_m(\eta)=\lim_{\alpha\to m}\left(\frac{J_\alpha(\eta)cos(\alpha\pi)-J_{-\alpha}(\eta)}{sin(\alpha\pi)}\right) \tag{A30}$$

where, m is an integer. Furthermore, the coefficient of Gamma function needs to be updated

$$\Gamma=e^{-\lambda Fo}\left(C_{nm}+\int_{Fo'=0}^{Fo}g_{nm}{}^*(Fo')e^{\lambda Fo'}dFo'\right) \tag{A31}$$

$$C_{nm}=\frac{\int_{\delta_r}^{1}\Phi d\eta\left(\sum_{k=1}^{n}r_k\int_{\xi_k}^{\xi_{k+1}}\psi_k d\xi\right)}{\int_{\delta_r}^{1}\Phi^2 d\eta\left(\sum_{k=1}^{n}r_k\int_{\xi_k}^{\xi_{k+1}}\psi_k{}^2 d\xi\right)} \tag{A32}$$

The rest of the solution is similar to that of Cartesian coordinate presented in Ref. [48]. A code is developed in MATLAB that calculates the eigenvalues and eigenfunctions in η and ξ (non-dimensional) coordinates as well as Gamma function as a function of Fourier number (dimensionless time). The closed-form of the dimensionless transient 2-D temperature domain is found in a series form as follows:

$$\theta(\eta,\xi,Fo)=\sum_{n=1}^{\infty}\sum_{m=1}^{\infty}\Phi_n(\eta)\psi_{nm}(\xi)\Gamma_{nm}(Fo) \tag{A33}$$

Our study indicates that the first term in eigenfunction Φ ($n=1$) and one term in eigenfunction ψ ($m=1$) yield the accuracy of 99% in the

temperature distribution calculation. Each run takes about 1.5 min on a 3.4 GHz PC.

Appendix B. . Uncertainty analysis

The uncertainty in the calculation of evaporative cooling energy and desorption energy is obtained based on the method proposed by Moffat [56], as follows:

$$\left(\frac{\delta Q_{evap}}{Q_{evap}}\right)^2 = \left(\frac{\delta \dot{m}}{\dot{m}}\right)^2 + \left(\frac{\delta \Delta T}{\Delta T}\right)^2 + \left(\frac{\delta \Delta t}{\Delta t}\right)^2 = 0.005^2 + \left(\frac{0.15\sqrt{2}}{2}\right)^2 + \left(\frac{\sqrt{2}}{1200}\right)^2 = 0.01125 \tag{B1}$$

$$\left(\frac{\delta Q_{des}}{Q_{des}}\right)^2 = \left(\frac{\delta \dot{m}}{\dot{m}}\right)^2 + \left(\frac{\delta \Delta T}{\Delta T}\right)^2 + \left(\frac{\delta \Delta t}{\Delta t}\right)^2 = 0.007^2 + \left(\frac{0.15\sqrt{2}}{3.2}\right)^2 + \left(\frac{\sqrt{2}}{1200}\right)^2 = 0.00439 \tag{B2}$$

Specific cooling power (SCP) is defined as the ratio of evaporative cooling energy to the product of cycle time and dry sorbent mass, Eq. (B3). The coefficient of performance (COP) is defined as the ratio of evaporative cooling energy to the desorption energy, Eq. (B4).

$$SCP = \frac{Q_{evap}}{m_{sorb}\tau_{cycle}} \tag{B3}$$

$$COP = \frac{Q_{evap}}{Q_{des}} \tag{B4}$$

The uncertainty in SCP and COP calculation is as follows:

$$\frac{\delta SCP}{SCP} = \sqrt{\left(\frac{\delta Q}{Q}\right)^2 + \left(\frac{\delta m}{m}\right)^2 + \left(\frac{\delta \tau}{\tau}\right)^2} = \sqrt{0.01125 + \left(\frac{1}{600}\right)^2 + \left(\frac{1}{1200}\right)^2} = 0.106 \tag{B5}$$

$$\frac{\delta COP}{COP} = \sqrt{\left(\frac{\delta Q_{evap}}{Q_{evap}}\right)^2 + \left(\frac{\delta Q_{des}}{Q_{des}}\right)^2} = \sqrt{0.01125 + 0.00439} = 0.125 \tag{B6}$$

Appendix C. . Analysis of variance (ANOVA)

The analysis of variance (ANOVA) is a systematic method that can be used to evaluate the impact of design parameters on the performance by calculating the sums of square, level of contribution, F-statistic ratio and p-value [49]–[51]. First, we generate the sample points of variables, e.g. using the Box–Behnken design [52] with three levels of design parameters shown in Table 3. Since each variable has three levels, the degree of freedom is equal to 2. Based on the sample points generated by Box–Behnken design, the objective functions are evaluated using the analytical models, each objective function is shown by X_j. $\overline{X}_j$ represents the average of objective functions for each variable, and $\overline{X}$ indicates the average of $\overline{X}_j$ for all the variables. With these definitions, the sums of squares, mean squares, F-statistic ratio, and level of contribution (ρ) can be calculated as shown in Table C1. n_j shows the sample size in the jth group (or the number of variables). F-statistic ratio represents the variability between treatment or the ratio of (differences among the sample means) / (an estimate of the variability in the outcome). The greater the F, the more significant effect that parameter has as it can cause more variation.

To examine whether a variable has a significant impact on the objective function, the Null hypothesis is employed as follows.

H_0: Null hypothesis, which hypothesizes that all the means are equal: $\mu_1 = \mu_2 = \mu_3 \ldots = \mu_k$ (j = 1, 2, 3, …, k). If this hypothesis is true, then the variable does not cause significant variation as all the means are equal; thus, the variable has an insignificant impact on the objective function.

p-value $\leq \alpha$: Reject H0. The differences between some of the means are statistically significant, which means it has significant impact.

p-value $> \alpha$: The differences between the means are not statistically significant, which means it has negligible impact.

α = significance level (usually 0.05). It means that there is 5% chance that Null hypothesis was wrong and that parameter is significant.

The p-value can be calculated based on the F-statistic ratio, significance level (α), degree of freedom of the treatment for each variable and degree of freedom of errors, shown by $F_{\alpha,\ df1,\ dfE}$. MATLAB was used to obtain the p-values for $F_{\alpha,\ df1,\ dfE}$. The greater the F, the smaller the p-value.

Table C1
Sums of square, level of contribution (ρ) and F-statistic ratio in the ANOVA.

Variables	Sums of square (SS)	Degrees of freedom (df)	Mean squares (MS)	*F*	ρ (%)
b	$SSB = \sum n_j\left(\overline{X}_j - \overline{X}\right)^2$	*k*-1 = 2	*MSB* = *SSB*/(*k*-1)	*MSB*/*MSE*	*SSB*/*SST*
t_f		2			
t_s		2			
ϕ		2			
τ		2			
r_1, $H_c/2$		2			
Error (residual)	$SSE = \sum\sum\left(X - \overline{X}_j\right)^2$	*N*-*k* = 54–12 = 41	*MSE* = *SSE*/(*N*-k)		*SSE*/*SST*
Total	$SST = \sum\sum\left(X - \overline{X}\right)^2$	*N*-1 = 53			

References

[1] International Energy Agency, "Air conditioning use emerges as one of the key drivers of global electricity-demand growth," 2018.
[2] International Energy Agency, "The Future of Cooling," 2018.
[3] J. M. Pinheiro, S. Salustio, J. Rocha, A. A. Valente, and C. M. Silva, "Adsorption heat pumps for heating applications," Renew. Sustain. Energy Rev., vol. 119, no. April, p. 109528, 2019.
[4] W. Goetzler, R. Zogg, J. Young, C. Johnson, Alternatives to Vapor-Compression HVAC Technology, ASHRAE J. 56 (2014) 12.
[5] C. Formann, I. Muritala, R. Pardemann, B. Meyer, Estimating the global waste heat potential, Renew. Sustain. Energy Rev. 57 (2016) 1568–1579.
[6] X. She, et al., Energy-efficient and -economic technologies for air conditioning with vapor compression refrigeration: A comprehensive review, Appl. Energy 232 (October) (2018) 157–186.
[7] A. Sharafian, Waste heat-driven adsorption cooling systems for vehicle air conditioning applications, Simon Fraser University, 2015.
[8] M.O.M. Abdullah, I.A.I.A.W. Tan, L.L.S. Lim, Automobile adsorption air-conditioning system using oil palm biomass-based activated carbon: A review, Renew. Sustain. Energy Rev. 15 (4) (2011) 2061–2072.
[9] H. Demir, M. Mobedi, S. Ulku, A review on adsorption heat pump : Problems and solutions, Renew. Sustain. Energy Rev. 12 (2008) 2381–2403.
[10] Invensor, "Adsorption Chiller InvenSor LTC 90 e plus," 2020.
[11] Fahrenheit cooling innovations, "Technical data sheets," 2019.
[12] SolabCool, "SolabChiller," 2018.
[13] NISHIYODO KUCHOUKI CO. LTD (HIJC Inc.), "ADCM models," 2007.
[14] Mitsubishi Plastics, "Mitsubishi Plastics M-TYPE," 2015.
[15] Mayekawa (MYCOM), "AdRef-Noa, adsorption chillers with zeolite," 2020.
[16] EnergyStar, "ENERGY STAR Most Efficient 2020 — Central Air Conditioners and Air Source Heat Pumps," 2020.
[17] "Rooftop HVAC System for Coach and Transit, Athenia AM II Series," Corporate white paper from Ingersoll Rand, Thermo king, 2016. .
[18] "Rooftop air conditioning units for buses and coaches," Corporate white paper from Espar Heating Systems, 2013. [Online]. Available: https://www.eberspaecher-na.com/fileadmin/data/countrysites/EB_Kanada/images/AC310350_SpecSheet_WEB_READY_052913.pdf.
[19] J. Li, M. Kubota, F. Watanabe, N. Kobayashi, M. Hasatani, Optimal Design of a Fin-type Silica Gel Tube Module in the Silica Gel / Water Adsorption Heat Pump, J. Chem. Eng. Japan 37 (4) (2004) 551–557.
[20] A. Sapienza, S. Santamaria, A. Frazzica, A. Freni, Influence of the management strategy and operating conditions on the performance of an adsorption chiller, Energy 36 (2011) 5532–5538.
[21] M. Louajari, A. Mimet, A. Ouammi, Study of the effect of finned tube adsorber on the performance of solar driven adsorption cooling machine using activated carbon – ammonia pair, Appl. Energy 88 (3) (2011) 690–698.
[22] Q. W. Pan, R. Z. Wang, Z. S. Lu, and L. W. Wang, "Experimental investigation of an adsorption refrigeration prototype with the working pair of composite adsorbent-ammonia," vol. 72, 2014.
[23] C. Y. Tso, K. C. Chan, C. Y. H. Chao, and C. L. Wu, "Experimental performance analysis on an adsorption cooling system using zeolite 13X / CaCl 2 adsorbent with various operation sequences," vol. 85, pp. 343–355, 2015.
[24] S.W. Hong, S.H. Ahn, O.K. Kwon, J.D. Chung, Optimization of a fin-tube type adsorption chiller by design of experiment, Int. J. Refrig 49 (2015) 49–56.
[25] L.Q. Zhu, Z.W. Gong, B.X. Ou, C.L. Wu, Performance Analysis of Four Types of Adsorbent Beds in a Double-Adsorber Adsorption Refrigerator, Procedia Eng. 121 (2015) 129–137.
[26] A. Sharafian, C. McCague, M. Bahrami, Impact of fin spacing on temperature distribution in adsorption cooling system for vehicle A/C applications, Int. J. Refrig 51 (2015) 135–143.
[27] A. Sapienza, et al., An innovative adsorptive chiller prototype based on 3 hybrid coated / granular adsorbers, Appl. Energy 179 (2016) 929–938.
[28] Q.W. Pan, R.Z. Wang, L.W. Wang, D. Liu, Design and experimental study of a silica gel-water adsorption chiller with modular adsorbers, Int. J. Refrig. 67 (2016) 336–344.
[29] A. Frazzica, et al., Design, realization and testing of an adsorption refrigerator based on activated carbon / ethanol working pair, Appl. Energy 174 (2016) 15–24.
[30] B. Zajaczkowski, Optimizing performance of a three-bed adsorption chiller using new cycle time allocation and mass recovery, Appl. Therm. Eng. 100 (2016) 744–752.
[31] Z. Rogala, Adsorption chiller using flat-tube adsorbers – Performance assessment and optimization, Appl. Therm. Eng. 121 (2017) 431–442.
[32] V. Palomba, B. Dawoud, A. Sapienza, S. Vasta, A. Frazzica, On the impact of different management strategies on the performance of a two-bed activated carbon / ethanol refrigerator : An experimental study, Energy Convers. Manag. 142 (2017) 322–333.
[33] U. Bau, et al., Dynamic optimisation of adsorber-bed designs ensuring optimal control Constraints, Appl. Therm. Eng. 125 (2017) 1565–1576.
[34] K. Chan, C. Tso, C. Wu, C.Y.H. Chao, Enhancing the performance of a zeolite 13X / CaCl 2 – water adsorption cooling system by improving adsorber design and operation sequence, Energy Build. 158 (2018) 1368–1378.
[35] B. Golparvar, H. Niazmand, A. Sharafian, A. Ahmadian Hosseini, Optimum fin spacing of finned tube adsorber bed heat exchangers in an exhaust gas-driven adsorption cooling system, Appl. Energy 232 (September) (2018) 504–516.
[36] U. Bau and A. Bardow, "Pareto-optimal performance of one-bed adsorption chillers by easy-to- implement heat-flow-based control," Appl. Therm. Eng., vol. 159, no. February, p. 113590, 2019.
[37] M. B. Elsheniti, M. A. Hassab, and A. Attia, "Examination of effects of operating and geometric parameters on the performance of a two-bed adsorption chiller," Appl. Therm. Eng., vol. 146, no. September 2018, pp. 674–687, 2019.
[38] A. Freni et al., Characterization of Zeolite-Based Coatings for Adsorption Heat Pumps. SPRINGER BRIEFS IN APPLIED SCIENCES AND TECHNOLOGY, 2015.
[39] A. Freni, L. Calabrese, A. Malara, P. Frontera, L. Bonaccorsi, Silica gel micro fibres by electrospinning for adsorption chillers, Energy 187 (2019), 115971.
[40] H. Bahrehmand, M. Khajehpour, M. Bahrami, Finding optimal conductive additive content to enhance the performance of coated sorption beds: An experimental study, Appl. Therm. Eng. 143 (July) (2018) 308–315.
[41] A. Freni, F. Russo, S. Vasta, M. Tokarev, Y. Aristov, G. Restucci, An advanced solid sorption chiller using SWS-1L, Appl. Therm. Eng. 27 (2007) 2200–2204.
[42] B. Dawoud, P. Höfle, S. Chmielewski, Experimental investigation of the effect of zeolite coating thickness on the performance of a novel zolite-water adsorption heat pump module, in: Tenth international conference enhanced building operations, 2010, pp. 1–8.
[43] M. Verde, J.M. Corberan, R. de Boer, S. Smeding, Modelling of a waste heat driven silica gel/water adsorption cooling system comparison with experimental results, in: ISHPC conference, Padua, Italy, 2011, pp. 7–8.
[44] Y. Aristov, A. Sapienza, D. Ovoshchnikov, A. Freni, G. Restuccia, Reallocation of adsorption and desorption times for optimisation of cooling cycles, Int. J. Refrig 35 (2012) 525–531.
[45] A. Freni, L. Bonaccorsi, L. Calabrese, A. Caprì, A. Frazzica, A. Sapienza, SAPO-34 coated adsorbent heat exchanger for adsorption chillers, Appl. Therm. Eng. 82 (2015) 1–7.
[46] U. Wittstadt, et al., A novel adsorption module with fiber heat exchangers: Performance analysis based on driving temperature differences, Renew. Energy 110 (2017) 154–161.
[47] Z. He, et al., Study on the performance of compact adsorption chiller with vapor valves, Appl. Therm. Eng. 126 (2017) 37–42.
[48] H. Bahrehmand, M. Bahrami, An analytical design tool for sorber bed heat exchangers of sorption cooling systems, Int. J. Refrig 100 (2019) 368–379.
[49] O.J. Dunn, V.A. Clark, Applied Statistics: Analysis of Variance and Regression, Wiley, New York, 1974.
[50] J.H. Goodnight, F.M. Speed, Computing Expected Mean Squares, SAS Institute, Cary, NC, 1978.
[51] R.V. Hogg, J. Ledolter, Engineering Statistics, MacMillan, New York, 1987.
[52] G. Box, D. Behnken, Some new three level designs for the study of quantitative variables, Technometrics 2 (1960) 455–475.
[53] J.S. Arora, Introduction to Optimum Design (2004).
[54] A. Sharafian, S.M. Nemati Mehr, P.C. Thimmaiah, W. Huttema, M. Bahrami, Effects of adsorbent mass and number of adsorber beds on the performance of a waste heat-driven adsorption cooling system for vehicle air conditioning applications, Energy 112 (2016) 481–493.
[55] V. Gnielinski, New equations for heat and mass transfer in turbulent pipe and channel flow, Int. Chem. Eng. 16 (2) (1976) 359–368.
[56] R.J. Moffat, Describing the uncertainties in experimental results, Exp. Therm Fluid Sci. 1 (1988) 3–17.